

Atomistic mechanisms for the ordered growth of Co nano-dots on Au(788): comparison of VT-STM experiments and multi-scaled calculations

S. Rohart, G. Baudot, V. Repain, Y. Girard, S. Rousset *

*Groupe de Physique des Solides: Universités Paris 6 et 7, CNRS, UMR 75-88
FR 2437: Matériaux et Phénomènes Quantiques, 2 place Jussieu, 75251 Paris
Cedex, France*

H. Bulou, C. Goyhenex

*Institut de Physique et Chimie des Matériaux de Strasbourg, UMR 75-04, 23 rue
du Loess, 67037 Strasbourg, France*

L. Provile

*Service de Recherches de Métallurgie Physique CEA/Saclay, 91191 Gif sur Yvette
Cedex, France*

Abstract

Hetero-epitaxial growth on a strain-relief vicinal patterned substrate has revealed unprecedented 2D long range ordered growth of uniform cobalt nanostructures. The morphology of a Co sub-monolayer deposit on a Au(111) reconstructed vicinal surface is analyzed by Variable Temperature Scanning Tunneling Microscopy (VT-STM) experiments. A rectangular array of nano-dots (3.8 nm x 7.2 nm) is found for a particularly large deposit temperature range lying from 60 K to 300 K. Although the nanodot lattice is stable at room temperature, this paper focus on the early stage of ordered nucleation and growth at temperatures between 35 K and 480 K. The atomistic mechanisms leading to the nanodots array are elucidated by comparing statistical analysis of VT-STM images with multi-scaled numerical calculations combining both Molecular Dynamics for the quantitative determination of the activation energies for the atomic motion and the Kinetic Monte Carlo method for the simulations of the mesoscopic time and scale evolution of the Co submonolayer.

Key words: Cobalt, gold, growth, Surface diffusion, vicinal single crystal surfaces, Molecular Dynamics, Monte Carlo simulations, Scanning tunneling microscopy
PACS: 68.55.-a, 68.47.De, 82.20.Wt, 68.37.Ef, 81.07.-b, 81.16.Dn

1 Introduction

Nucleation and growth of mono-disperse nanostructures is a challenging field both for theoretical modeling and practical applications due to their new magnetic, electric and catalytic properties. Growth of regular islands has been achieved in various systems such as metal aggregates supported on insulator surfaces [1,2], hetero-epitaxial growth of semiconductors including self-assembled quantum dots [3,4], and metal on metals systems [5,6]. Although nucleation and growth models have been extensively developed and compared with experiments in the case of homogeneous substrates, growth on heterogeneous substrate has been considered only recently. The hetero-epitaxial growth of highly strain islands is still very difficult to modelize, but simple systems have been considered such as nucleation on substrates containing point-defects traps [1,2,7] or spatial ordering of islands grown on patterned substrates [6,8]. The use of spontaneously nanostructured substrates as templates for organized growth is a promising way as it allows to grow not only regular nanostructures but also to grow high density lattice of regular nanostructures over macroscopic scales. This opens up the way for new studies of both individual and collective physical properties by means of standard averaging technics.

Metal on metal systems provide model systems for ordered growth on well-defined nano-patterned substrates [5,6,9]. Experimentally, this phenomena has been successfully applied to the formation of nanostructures but very few studies are dealing with the atomistic mechanisms leading to the organization and the quantitative determination of the associated energies. The precise determination of the atomistic mechanisms for a given substrate should allow to make some prediction to get an ordered growth with various deposited material and to find out the conditions (flux, temperature) for the narrowest size distribution. Indeed the use of a nanostructured template is not a sufficient condition to get an ordered growth. For example, the reason why Fe, Co, Ni, Cu [5,10,11,12] display an ordered growth on Au(111) at room temperature whereas Ag, Al [12,13,14] do not is still under debate.

In this paper we study the nucleation and growth of Co nanodots on a Au(111) reconstructed, vicinal substrate. This system has been shown recently [15,16,17] to display an improved long-range order and a narrower size distribution than on Au(111). Using a Variable Temperature Scanning Tunneling Microscope (VT-STM), we have studied the evolution of the growth morphology with temperature. With a statistical analysis of the STM images combined with Kinetic Monte Carlo (KMC) simulation and Molecular Dynamics (MD) calculation, we determine the mechanisms at the origin of the organization of Co

* Corresponding author

Email address: rousset@gps.jussieu.fr (S. Rousset).

URL: <http://ufrphy.lbhp.jussieu.fr/nano/> (S. Rousset).

nanodots on Au(788). This result opens the way to make quantitative predictions about the ordered growth of other materials on Au(788) like Fe or Ni.

2 Experimental Details

The Au(788) substrate is a stable, vicinal surface misoriented by 3.5° with respect to the (111) plane toward the [-211] azimuth. It has been fully presented in a previous paper [15]. Its surface displays a very regular succession of monoatomic steps and 3.8 nm wide terraces. Due to the $22 \times \sqrt{3}$ reconstruction of the Au(111) plane, Au(788) is also structured in the direction perpendicular to the steps (7.2 nm periodicity). It was shown in earlier studies that this surface can be used as a template for the growth of cobalt nano-dots [18,15,16,17] as the crossing of a discommensuration line and a step edge acts as a favored nucleation site.

Our Au(788) sample is a Au single crystal cut by spark erosion to produce a 4 mm diameter and 2 mm thick disk. It was prepared in a UHV chamber (base pressure 3×10^{-11} mbar) using repeated argon sputtering (5×10^{-6} mbar Ar pressure, 1 keV energy) followed by 850 K annealing cycles.

The cobalt is evaporated from a 2 mm diameter cobalt rod directly heated by electron bombardment ($I_{em} = 12$ mA, $HV = 1$ kV). The pressure during this process is always below 2×10^{-10} mbar. The flux rate is about 0.2 ML per minute. The uncertainty on the absolute cobalt coverage is about 20%. Deposition was achieved directly under a VT-STM. For temperatures below room temperature, STM images were taken at the growth temperature in order to be sure that no change could be introduced by the annealing. For deposition temperatures above room temperature, STM images were taken at room temperature as cooling down the sample does not change the result (clusters density, size distribution and clusters morphology).

3 VT-STM experiments

In order to determine the atomistic mechanisms at the origin of the ordered growth of Co on Au(788), we have performed STM images for different substrate temperatures and Co coverage. In a first part, we present and describe the STM images for temperature ranging from 35 K to 430 K. In a second part, we extract mean quantities from a statistical analysis of the images.

3.1 STM images

STM images of the Co deposition on Au(788) at different temperatures are presented in figure 1. Roughly, three different regimes are found: first, for low temperatures (below 60 K, see fig. 1a) no order is found: small clusters are randomly dispersed on the surface and the clusters density is very high. The inset of fig. 1a shows a low Co coverage image, where single Co adatoms can be seen. We can notice that the positions of these adatoms seem not to be influenced by the surface structuration (steps, discommensuration lines). At 65 K (fig. 1b), an organization clearly appears. However, many islands are still randomly located on the surface. Above 65 K, the quality of the organization improves a lot. Few evolution is seen versus the temperature: the same result is obtained from 95 K to 170 K. In the inset of 1c, we can see that dots are located near the crossing of a discommensuration line and a step edge. We call these sites "favored nucleation sites". As a consequence an array of pairs of dots placed on a rectangular lattice is formed on the surface. This array displays a long range order as there is exactly one dot on every favored site. Only few defects (missing dot, dot in a non preferential surface site...) can be seen, which shows the quality of the array. From 170 K to 300 K the order remains but it is not as good as in the previous temperature range and an increasing number of defects (missing dots, coalesced neighboring dots) can be seen. From 200 K to 300 K, low Co coverage images show that many Co atoms are inserted in the gold surface layer in preferential atomic sites located near the step edges and the discommensuration lines (cf. inset of fig 1e). For temperatures higher than room temperature, it has been shown [15,16] that the order disappears. We can see on fig. 1f that the growth result is a few, big, faceted clusters randomly distributed on the surface.

The size distributions for different substrate temperatures are presented in figure 2. These size distributions were performed with an object processing software on several images (five to ten 60 nm wide STM images i.e. 1000 to 2000 dots). At low temperature (40 K in the figure 2a), the size distribution does not show a maximum and the smallest clusters are the most often found. For higher temperatures (95 K and 135 K, figures 2b and c), the size distributions show a maximum. Moreover, in the 95 K - 170 K range, the width at half maximum decreases when temperature increases and rather good mono-disperse size distributions are obtained above 135 K. It is worth to notice that an annealing to room temperature increases dramatically the quality of this size distribution [15,17]. At 300 K, the size distribution shows that two kinds of dots co-exist on the surface: some small ones (less than 20 atoms) and some greater ones (more than 100 atoms). This is in agreement with the STM image shown in figure 1e which reveals lots of inhomogeneities. The origin of these inhomogeneities will be discussed later with the help of the KMC simulations.

3.2 Critical density study

For every substrate temperature (40 K - 480 K), cobalt deposition was done step by step in order to record the evolution of the growth morphology with the coverage. We have extracted from these images the Co clusters density as a function of the coverage. Some of these curves for several temperatures are presented in figure 3. This evolution reflects the well-known scenario of the sub-monolayer growth on surfaces (see for example [19] or [20]). At the beginning the density of clusters increases regularly as the adatoms nucleate new clusters. Then the density of clusters stabilizes and the size of the clusters increases: in this regime the density is constant and is called the critical density (n_c). For higher coverage, the coalescence regime is reached and the density decreases.

Several studies [19,21,22,23,24] have already pointed out the importance of the critical clusters density (i.e. the maximum cluster density versus the coverage.), which reflects the diffusion length of adatoms on the surface, to elucidate the growth mechanisms.

The evolution of the critical cluster density versus the temperature is given in figure 4 in a standard Arrhenius plot. This curve gives a quantitative analysis of the STM images presented before. It displays a large range of temperature (60 K - 300 K) where the density of clusters is nearly constant. This clearly shows that the growth is not homogeneous on the Au(788) surface which is explained by the nano-patterning of the surface. We can remark that the density equals the density of favored nucleation sites, which is in agreement with STM images described above (fig. 1c and d). Once more the curve clearly shows that the quality of the dot array decreases above 160 K as the clusters density slowly decreases until 300 K as pointed out above. Under 60 K and above 300 K, the strong linear decrease of the logarithm of the clusters density as a function of $1/k_B T$ is typical of nucleation and growth on homogeneous surfaces [24]. This indicates that the growth is less influenced by the favored nucleation sites.

4 Interpretation and multi-scaled calculations

We have demonstrated that Co displays an ordered growth on Au(788) in a large temperature range (60 K - 300 K). As a comparison, one can see that it is particularly larger than the plateau found by H. Brune et al. [6] for the organized growth of Ag nanodots on Ag bilayer on Pt(111) (100 K - 130 K). In this case the organized growth was due to a confinement of the adatoms by the dislocation lines of the strain-relief pattern. The organized regime stops

as soon as the adatoms have sufficient energy to cross these lines. We wonder which atomistic mechanisms are at the origin of the ordered growth on Au(788) and explain such a large temperature range.

4.1 A simple view of the organized growth

What are the pertinent parameters, which explains the temperature range for an ordered growth regime ?

For low temperatures, the mean free path of adatoms on a surface is lower than the mean distance between favored sites (or the density of cluster is higher than the density of favored sites as it can be seen on fig. 4). In consequence, the adatoms cannot be influenced by the periodic patterning of the surface as its period is wider than the region explored by adatoms. That is why no order is found for a growth with such substrate temperatures. We can estimate the temperature threshold (T_o) over which the system displays an ordered growth as the temperature at which the diffusion length of the adatoms on an hypothetical homogeneous substrate equals the mean distance between two favored sites. As a consequence, the parameters that determine the beginning of the ordered growth regime are the diffusion energy E_{diff} and the mean distance between favored nucleation sites l_t (or, what is more convenient, the density of favored sites $n_t = 1/l_t^2$).

Using the well-known Rate Equation (RE) model for homogeneous growth [21,23,24,25], we estimate the lowest temperature T_o , for which the ordered growth regime is reached for Co on Au(788). We assume that all dimers are stable on the surface (critical cluster size $i^* = 1$), as for low temperature the dimer cohesion energy is much higher than the thermal energy. The evolution of the critical clusters density with temperature is given by:

$$\begin{aligned} n_c &= \eta(D/\sigma F)^{-1/3} \\ &= \eta(D_0/\sigma F)^{-1/3} \exp(E_{diff}/3k_B T) \end{aligned} \quad (1)$$

with η a fixed prefactor (about 0.25 using the lattice approximation for capture rates [24]), F the deposition rate (Flux), D_0 the diffusion coefficient at 0 K, σ the size of a lattice site and E_{diff} the diffusion energy. The ordered growth regime is reached when the clusters density equals the density of favored sites (n_t). Taking $n_c = n_t = 1/200$ the ratio of favored sites per atomic sites, $E_{diff} = 0.12$ eV [26,27] and $D_0 = 5.8 \times 10^{12}$ Å²/s [28] and $\sigma = 7.2$ Å² we find that an ordered growth should be observed for temperatures over 83 K, which is a little higher than the experimental value ($T_o^{STM} = 70$ K). As we know that the RE model given in equation eq. 1 tend to over estimate the dot

density [23], we find that there is a good agreement between this qualitative estimation and STM experiments.

For temperatures above T_o , some atoms are trapped into the favored sites and we observe an ordered growth regime. A characteristic of such a regime is that the critical clusters density is constant with temperature and equals the density of favored sites. Indeed the diffusion length of the adatoms is limited by the presence of the favored sites. This ordered growth occurs as long as the typical energy of the trapping mechanism is sufficient to stabilize adatoms in the favored sites. We call T_e the last temperature for which an ordered growth is observed. The most important parameter, which determine T_e is the energy barrier for an atom to jump out of the trap E_t .

In order to estimate T_e , we modify the RE model for homogeneous growth to take into account the favored sites, following the idea of J. Venables in [7,29]. Assuming for simplicity that dimers are stable on the surface (the dimers binding energy is infinite), the RE for the homogeneous growth describe the evolution of the population of adatoms n_1 and stable island n_x . In this new model, we add an homogeneous distribution of traps with the density n_t . We then need to consider the evolution of the population of trapped adatoms n_{1t} and trapped stable islands n_{xt} . The evolution of n_{1t} is mainly given by the rate for an adatom to reach a trap $\sigma_1 D n_1 n_{te}$ and by the rate for this atom to jump out of the trap $n_{1t} \nu_0 \exp(-E_t/k_B T)$ [29]. σ_1 is the capture rate of trap (which is assumed for simplicity to be equal to the capture rate of an adatom), D is the diffusion coefficient ($D = D_0 \exp(-E_{diff}/k_B T)$), n_{te} is the density of empty traps ($n_{te} = n_t - n_{1t} - n_{xt}$), ν_0 is the attempt rate and E_t is the energy barrier for the jump. The four rate equations for the evolution of n_1 , n_{1t} , n_x and n_{xt} are given by :

$$\left\{ \begin{array}{l} \frac{dn_1}{dt} = F - \sigma_1 D n_1 (2n_1 + n_{te} + n_{1t}) - \sigma_x D n_1 (n_x + n_{xt}) + n_{1t} \nu_0 \exp(-E_t/k_B T) \\ \frac{dn_{1t}}{dt} = \sigma_1 D n_1 (n_{te} - n_{1t}) - n_{1t} \nu_0 \exp(-E_t/k_B T) \\ \frac{dn_x}{dt} = \sigma_1 D n_1^2 \\ \frac{dn_{xt}}{dt} = \sigma_1 D n_1 n_{1t} \end{array} \right. \quad (2)$$

A key parameter of these equations is the capture rates for an adatom (σ_1) and a stable cluster (σ_x). The choice for the values is discussed by H. Brune in [24]. We take $\sigma_1 = 3$ and $\sigma_x = 7$, which was found to give a good agreement for low coverages. In these equations, we neglect the possibility of direct impingement of a deposited atom onto monomeres or islands. The numerical integration of these equations allows us to determine the evolution of the cluster density on the surface. Taking E_t as a free parameter, the figure fig.5 gives the best fit of the experimental data for the evolution of the cluster density with the temperature. With $E_t = 0.82$ eV, the model in eq.2 reproduce very well the

position of the end of the plateau with $T_e \simeq 300$ K. This result is consistent with previous theoretical [7,29] and experimental studies of the growth of *Pd* on *MgO* [1] and *Fe* on *CaF₂* [2] where point defects on the surface trap the adatoms on the surface with leads to a favored nucleation on the point defects.

These RE calculation gives an estimation of the key parameters involved in the growth of Co on Au(788). However, in order to go further than the mean-field approximation and to take into account more complex mechanisms we perform KMC simulations together with MD calculations for the quantitative determination of the activation energies of the mechanisms involved in the KMC.

4.2 Multi-scaled calculations

4.2.1 Principle of the calculations

The KMC modeling is a powerful tool for studying the time evolution of the growth of atom clusters over the time scale of diffusion and for mesoscopic space scale. About theory of the KMC for the growth of thin film, the reader can refer to the works of P. Jensen in [20] and H. Brune in [24]. The comparison between the STM images and the simulations gives an accurate insight about the atomic mechanisms that yield the ordered growth of Co nanodots.

We have developed a KMC code based on the algorithm of Bortz, Kalos and Lebowitz [30]. The surface is modeled by an array of adsorption sites placed on an hexagonal lattice. Each of this site represents an atomic position where a Co atom may reach a local mechanical equilibrium. The atomic displacements between those sites are ruled by the transition state theory:

$$p_i = \nu_0 \exp(-\Delta E_i/k_B T) \quad (3)$$

The attempt frequency ν_0 is fitted so that the KMC model reproduce the correct diffusion coefficient D_0 given in [28]. We then have $\nu_0 = D_0/(4\sigma)$ with σ the surface of an atomic site ($\sigma = 2.88 \times 2.88\sqrt{3}/2 = 7.2 \text{ \AA}^2$).

ΔE_i is the energy barrier for the atomic processes. In principle the number of different barriers is very large, and their exact values are unknown. Only approximate total energy methods can at present give results for all the processes of interest here. We have used the Quenched-Molecular-Dynamics (QMD) to give us an idea about the important processes. QMD is an energy minimization procedure, based on the integration of the equation of motion for each atom in the system, which consists of canceling the velocity of the atoms when the product of the force acting on the atoms by their velocity becomes negative.

Then the kinetic energy of the system decreases leading to the minimization of the potential energy at 0 K [31,32]. In our calculations, the equations of motion are integrated with a velocity-Verlet integrator [33] with a time step of 5 fs which is the best compromise between calculation speed and system stability. We considered that the quenched situation is reached when the system temperature is lower than 3 mK which temperature fluctuations lower than 0.2 μ K/fs, which ensure an energy precision better than 0.1 meV.

The interatomic forces are calculated in the framework of the Second Moment Approximation of the Tight Binding Theory (TBSMA) [34] from the total energy

$$E_{tot} = \sum_i \left\{ \sum_{j \neq i} A_{X_i Y_j} \exp \left[-p_{X_i Y_j} \left[\frac{r_{ij}}{r_0^{X_i Y_j}} - 1 \right] \right] - \sqrt{\sum_{j \neq i} \xi_{X_i Y_j}^2 \exp \left[-2q_{X_i Y_j} \left[\frac{r_{ij}}{r_0^{X_i Y_j}} - 1 \right] \right]} \right\} \quad (4)$$

X and Y indicate the chemical species (Co,Au), r_0^{XX} the first-neighbour distance in the metal X and $r_0^{XY} = \frac{1}{2}(r_0^{XX} + r_0^{YY})$. The parameters A_{XY} , q_{XY} , p_{XY} , and ξ_{XY} (Table 1) are fitted to the experimental values of the cohesive energy, lattice parameter, and elastic constants [35,36] for homoatomic interactions ($Co - Co$, $Au - Au$). TBSMA potentials are known to underestimate surface energies. Then, a peculiar attention has been paid in order to reproduce the difference between the surface energies of Co and Au [26]. Heteroatomic interaction $Au - Co$ parameters are calculated by fitting the positive heats of solution for a single substitutional impurities and refined in order to reproduce the existence of a miscibility gap in the phase diagram of the bulk $Au - Co$ system [37].

Element	A (eV)	p	ξ (eV)	q	r_0 (Å)
Au-Au	0.189	10.40	1.744	3.87	2.880
Au-Co	0.140	10.63	1.656	3.11	2.695
Co-Co	0.106	10.87	1.597	2.36	2.510

Table 1

Parameter value for $Au - Au$, $Au - Co$, and $Co - Co$ interactions

Calculations have been performed on an Au(111) slab consisting of two terraces, each of them containing ($10 \times 15 \times 8$) gold atoms, plus one cobalt adatom, with periodic boundary conditions in the directions $\langle 1\bar{1}0 \rangle$ and $\langle \bar{1}\bar{1}2 \rangle$ parallel to the surface. The dimension of the terraces along the $\langle \bar{1}\bar{1}2 \rangle$ has been set in order to reproduce the dimensions of the Au(788) terraces.

The determination of the relevant processes needs to calculate the activation energy of the different possible mechanisms, i.e. by calculating the energy of the system along the minimum energy path between initial and final states.

The problem of finding the minimum energy path for an adatom diffusion from an equilibrium site to another one on simple surfaces, such as Au(111) for example, is straightforward since it is a straight line between the initial and final state. In the case of more complex surfaces, such as vicinales and reconstructed ones, the problem is more difficult, in particular, near steps and discommensurations, since in these cases, the minimum energy path is no longer a straight line between initial and final equilibrium sites. The most reliable method is then to perform precise mappings of the adsorption energies of the Co adatom on selected area and then to apply a path finding algorithm.

Figure 6 display the energy map of a Co adsorption in the step area. For each point, only the Co (x,y)-coordinates are strained at fixed values during the quenching procedure. The step of the mappings has been set to 0.100 Å along the $\langle 1\bar{1}0 \rangle$ direction and 0.087 Å along the $\langle \bar{1}\bar{1}2 \rangle$ direction. The Dijkstra's path finding algorithm has been applied in order to determine the minimum energy path [38].

Searching for simplicity, among numerous atomistic events that have been tested by the Molecular Dynamic, very few of them have been selected for the KMC simulations. The dependence of ΔE_i is represented by $\Delta E_i = E_{diff} + n.E_{Co-Co} + \delta_{loc}$ where n is the number of Co first neighbors and δ_{loc} is zero over the all surface but for some specific sites where the Co energy landscape is locally modified because of the heterogenities of the substrate. The numerical values of parameters are given in table 2. The quantity δ_{loc} describes the energies in specific sites and will be given further as ΔG_{ads} , ΔG_{ex} , ΔE_{ex} . The number of atomic events and consequently the number of parameters are reduced to a minimum in order to stress the driving mechanisms. The surface diffusion barrier reported in fig. 6 ($E_{diff} = 0.15$ eV) is higher than the one reported in Ref. [26] ($E_{diff} = 0.12$ eV). The origin of such a discrepancy comes from the fact that in Ref. [26], the calculations have been performed on a $22 \times \sqrt{3}$ reconstructed surface ; in this case the stress relief induced by the reconstruction lowers the diffusion energy of adatoms [39,40,41]. We take $E_{diff} = 0.12$ eV, which should be more correct for our problem.

Parameter	Value
ν_0	3.28×10^{12} Hz
E_{diff}	0.12 eV
E_{Co-Co}	0.44 eV

Table 2

KMC parameters obtained by mean of Molecular Dynamic calculations. The attempt rate ν_0 is calculated from ref. [28] and the diffusion energy E_{diff} can be found in [26,27].

For the KMC simulations, the surface is 500×500 site wide with periodic

boundary conditions. The deposition is treated as a random event which has a probability that is adjusted with respect to the deposition rate as suggested in [20].

A KMC simulation with no specific sites, i.e., of a deposition on a virtual homogeneous surface with the parameters of table 2 is done to compare our KMC model with the RE model for homogeneous nucleation [21,24]. The variation of the critical cluster density with the temperature is shown in fig.7c. A good agreement has been found for the two growth regimes:

First, for the low substrate temperatures, the cluster density does not depend on the temperature: this is the "post-nucleation" regime [24] (critical cluster size $i^* = 0$) where the adatoms diffusion is negligible compared to the deposition rate.

Second, for high temperatures the critical cluster density is given by eq.1. This is a regime with a critical cluster size $i^* = 1$, where the diffusion of adatoms is significant and where dimers are stable. Using eq.1, a fit of the numerical data from KMC enables us to deduce the diffusion energy. We find 120 ± 2 meV while the input E_{diff} was 120 meV which reveals a good agreement.

For simplicity, the influence of the Schwoebel barriers yielded by the surface steps on the adatoms diffusion is neglected in our model. This approximation is vindicated by the fact that the presence of the favored adsorption sites lessens the mean free path of the adatoms which is actually lower than the steps width as long as we have an ordered growth. Indeed, the steps have roughly no influence over the organization while the adatoms mean free path is smaller than the steps width. For higher temperature, i.e. for temperature higher than T_e , the mean free path of adatoms is longer than the steps width. However, as this appends for temperatures above than T_e (about 300 K), the steps are not of a great influence on the diffusion as the energy of the Schwoebel barrier (0.4 eV) is much lower than the energy of the adatoms to leave the favored sites (about 0.8 eV). The temperature threshold above which the steps are expected to play a role has been estimated by testing a KMC simulation with a virtual surface whose the steps involve an infinite Schwoebel barrier. It was found that the temperature threshold is higher than T_e which indicates that our approximation is valid in order to give a good description of the ordered growth regime.

The effect of the discommensuration lines is simplified by introducing a set of favored sites on the KMC model surface. Each of those sites is located near the step edge (the possibility of a repulsive diffusion barrier to cross the discommensuration line as suggested in [26] is neglected). According to the atomically resolved STM images [15] of the structure of Au(788) which show inserted Co atoms in the gold surface layer, two favored sites are separated

by 7 atomic sites in a dense direction and the density of the favored sites is 1/200.

In the favored sites, two different mechanisms can be considered: first a favored adsorption, which was foreseen by MD calculation on the discommensuration line on a Au(111) surface in [26] and second an exchange of the adsorbed Co atom in place of the underlying Au atom, which was observed by atomically resolved STM [15]. The favored adsorption mechanism involves only one additional parameter to the homogeneous surface parameters: the energy gain of the adatom in the site ΔG_{ads} measured with respect to a normal adsorption site (see position 3 in fig.8a). The exchange mechanism is described with two additional parameters: the activation barrier for the exchange ΔE_{ex} and the energy gain of the atom ΔG_{ex} when it is inserted in the gold surface layer (see position 4 in fig.8a). The three additional parameters have been estimated by MD calculations. Figure 8b displays the minimum energy path for a Co-Au exchange near the step. Only the Co z-coordinate has been strained during the quenching procedure.

4.2.2 Choice of the mechanisms for the ordered growth

In order to prove the need for the two mechanisms described above, we test successively the KMC simulations with only one of the two mechanisms. A first try with the favored adsorption mechanism leads to $\Delta G_{ads} = 0.7$ eV in order to fit the thermal variation of the maximum cluster density. A qualitative agreement between the experiment and the KMC simulations is found. This simulation is very close to the RE calculation described above as they both correspond to the same mechanism. The best fit is obtained with the same energy barrier to leave the favored site ($G_{ads}^{KMC} + E_{diff} = E_t = 0.82$ eV) in both KMC and RE calculation. It is worth noticing that the fit for low temperature is better with KMC than with the RE model. The temperature T_o is particularly well reproduced with this model ($T_o^{KMC} \simeq 75$ K, $T_o^{STM} \simeq 70$ K). The end of the plateau is much better reproduced by KMC than by RE calculation. This is due to the influence of the dimer bonds: in RE calculation the possibility for a dimer to break is neglected although the dimer binding energy (0.52 eV) is small with respect to the temperatures in the end of the plateau (around $T = 300$ K).

However, the value of $\Delta G_{ads} = 0.7$ eV cannot be explained by a favored adsorption mechanism. Indeed, this value is in strong contradiction with the MD calculations, which indicates a value of 0.1 eV [26] on a flat reconstructed surface. Although the presence of the step is not included in the MD calculation of [26], the correction is not expected to be so large. Such a value should correspond to a more complex mechanism, such as a place exchange.

We test this hypothesis with a KMC simulation with the favored place-exchange alone. The energy barrier to reach the favored site is fixed to $\Delta E_{ex} = 0.32$ eV so that the place exchange does not occur before 200 K according to the VT-STM experiment. The gain of the Co atom when it is inserted is $\Delta G_{ex} = 0.5$ eV and thus the energy to leave the favored sites is 0.82 eV. In the limits of the explored temperature range, we have only seen few deviation of the growth regime from the growth on an homogeneous growth. The small deviation at about 200 K is explained by the activation of the favored place exchange mechanism. The qualitative disagreement can be explained as follows: when the adatoms have sufficient energy to diffuse on a distance equal to the mean distance between favored sites, their thermal energy is still too low to enable them to reach the favored site, due to the access barrier ΔE_{ex} (we can remark that this value is very low in comparison to typical values for the place exchange on a flat, unreconstructed surface). As a consequence, the density keeps on decreasing as the favored sites cannot play any role. When the thermal energy of the adatoms overpass the place exchange barrier then the nucleation becomes heterogeneous but there is still less than one dot per favored site. We can conclude that the favored place exchange mechanism cannot explain alone the experimental results. This is consistent with our low coverage images for various temperatures which do not show the place exchange mechanism below 200 K.

4.3 Interplay between adsorption and place exchange mechanisms.

4.3.1 Final model

A realistic fit of the experimental data is achieved with the combination of the two mechanisms inside the favored sites. The thermal variation of the critical cluster density fig.9 is found with the parameters that are summarized in the table 3. This table gives also a set of parameters calculated by QMD. These parameters are calculated on various surfaces as we do not know precisely the atomic structure of the Au(788) surface. This allows us to make a comparison with the parameters found in KMC calculations. The adsorption gain ΔG_{ads} was found to be 0.28 eV in KMC. This high value with respect to the KMC must be due to the influence of the step edge. Indeed, on the discommensuration line on the Au(111) surface, every sites along the line is equivalent. This is not the case on the Au(788) surface which indicates that the step edge changes the adsorption energies and make a more favorable site. The values found by the QMD for the exchange mechanism are of the same order as the values of the KMC although the discommensuration lines is not included in this calculation. The fact that the exchange takes place at a precise is due to kinetic effect. Indeed the exchange and the favored adsorption take place at the same place. The adsorption gain in this site increases the residence time

of the adatoms on this sites which increases the exchange probability in the same way.

Parameter	KMC	Molecular Dynamic	
		Au(788)	Au(111)
		non reconstructed	reconstructed
E_{diff}	0.12 eV	0.15 eV	0.12 eV
ΔG_{ads}	0.28 eV		0.10 eV
ΔG_{ex}	0.78 eV	0.60 eV	
ΔE_{ex}	0.32 eV	0.36 eV	

Table 3

KMC parameters for the favored adsorption and the exchange mechanisms to fit the experimental data. For comparison various MD parameters are given. Calculation were done on a Au(788) non reconstructed surface and on a Au(111) reconstructed surface (see [26,42]). The exchange on the Au(788) surface was performed at 1 rows of the step edge. The exchange and adsorption on Au(111) were performed on the top of the discommensuration line.

A plateau with exactly one dot per favored site is found in the temperature range which lies from 75 K to 150 K. This plateau can only be explained with the favored adsorption mechanism as no place exchange occurs for so low temperatures. The KMC images shown in figure 10 are in good agreement with STM experiments and confirm that the best condition for a long range order with a narrow cluster size distribution is a sample temperature around 130 - 150 K.

Above 150 K, the energy gain is no more sufficient to stabilize the adatoms and the clusters density decreases. Above 200 K, the place exchange becomes efficient in the simulations, so the cluster density stops to decrease and a rough organization is maintained up to 300 K, i.e., the ratio n_c of the number of cluster per favored sites is such as $1 < n_c < 2$. The most important point is that in this temperature range, the order is still present on the surface (see fig. 10c) but the number of defect (empty favored site, coalesced neighbor dots...) is more important than in the previous regime. This fact is particularly evident for the simulation at $T = 300$ K, i.e. the bimodal size distribution is pretty well reproduced. The origin of this size distribution is the weakness of the bonds between the Co atoms. As a consequence, the critical size (biggest unstable cluster) of a cluster on a favored site is 2. This explains why the growth of the dots in the favored sites is strongly inhomogeneous: some dots grow faster and lead to big clusters when they coalesce with the neighboring cluster.

One may wonder why in the 200 K - 300 K temperature range there is an organization whereas in the simulation including only the exchange mechanism

with the same parameters we do not find any organization in the same temperature range. This can be explained by the fact that the evolution of the cluster density is not simply explained by the sum of two different mechanisms but a combination. Above 200 K, even if the favored sites cannot stabilize adatoms with just the favored adsorption mechanism, the residence time of the adatoms is increased in these sites, with respect to the normal sites. As a consequence, the exchange probability is increased in the same way.

4.3.2 Discussion

This interplay between the two mechanisms is a key which explains the large temperature range for the organized growth. Indeed place exchange mechanism is not favorable for the organized growth due to the large place exchange barrier but provide a strong energy gain in the favored site. On the opposite, the favored adsorption mechanism lead to the organization but the low energy gain cannot maintain an organization in a large temperature range. The good combination of these two mechanisms provides the organization for a large temperature range. We have determined the four pertinent parameters E_{diff} , ΔG_{ads} , ΔE_{ex} and ΔG_{ex} in our system. In order to generalize this model to other systems, we now discuss which relation are required for these parameters in order to obtain an ordered growth for a large temperature range.

First of all, the width of the ordered growth regime is determined by E_{diff} for the temperature T_o and by $E_t = \Delta E_{ex} + \Delta G_{ex} - \Delta G_{ads}$, the energy barrier for the removal process of the place exchange (when a Au adatom exchanges with a Co inserted atom), for the temperature T_e . A key to obtain a regular organization on the whole temperature range is the interplay between the two mechanisms. As a consequence, the removal process for the adsorption mechanism should not occur before the place exchange is possible. From an energetic point of view this means that the gain of the favored adsorption mechanism ΔG_{ads} must be higher or of the same order than the place exchange barrier ΔE_{ins} . However the absolute value of these energies is not a key as the temperature at which the interplay occurs is not very important. In the case of Co on Au(788) ΔG_{ads} is just of the order of ΔE_{ins} . That is why we only have a rough organization in the 170 K - 300 K temperature range. As the interplay between the two mechanisms is not perfect, we can see a small "accident" in the evolution of the critical clusters density with temperature (see fig. 9).

5 Conclusion

The ordered growth of Co nanodots on the Au(788) surface is proved to be due to the presence of favored site where two microscopic mechanisms occur:

a favored adsorption and a place exchange mechanism. The combination of these two mechanisms leads to the organization of the Co nanodots for a temperature that ranges from 60 K to 300 K. A rectangular array of mono-disperse cobalt nanodots is then yielded with a great regularity. These experimental results open the way to study the physical properties of nano-sized ferromagnetic particules with integrating technics like Magneto-Optical Kerr Effect. With such a mono-disperse array of nanodots integrating technics can be used to deduce the physical properties of a single particle.

The numerical simulations, in spite of many approximations, provide us an accurate insight about the fundamental mechanisms of the growth of Co/Au(788). A mechanism at the origin of the organized growth is a place exchange. For that kind of mechanism, the removal process is very hard as it corresponds to an atomic rearrangement in the surface layer. It was found to be helped by a favored adsorption mechanism. Indeed, due to the energy gain of the adatoms in these sites, the place-exchange probability is increased because the mean residence time of atoms is large. This explains why the growth of Co on Au(788) is organized with a so large temperature range. Further experiments and calculations about the deposition of other materials on Au(788) should be of interest to confirm our nucleation and growth scenario.

We gratefully acknowledge C. Priester and G. Prevot for the enlightening discussions.

References

- [1] G. Haas, A. Menck, H. Brune, J. Barth, J. Venables, and K. Kern, *Phys. Rev. B* **61**, 11105 (2000).
- [2] K. Heim, S. Coyle, G. Hembree, and J. Venables, *J. Appl. Phys.* **80**, 1161 (1996).
- [3] J. Tersoff, C. Teichert, and M. Lagally, *Phys. Rev. Lett.* **76**, 1675 (1996).
- [4] C. Teichert, *Phys. Rep.* **365**, 335 (2002).
- [5] D. Chambliss, R. Wilson, and S. Chiang, *Phys. Rev. Lett.* **66**, 1721 (1991).
- [6] H. Brune, M. Giovannini, K. Bromann, and K. Kern, *Nature* **394**, 451 (1998).
- [7] J. Venables, P. Bennett, H. Brune, J. Drucker, and J. H. Harding, *Phil. Trans. R. Soc. Lond. A* **361**, 311 (2003).
- [8] C. Lee and A. Barabási, *Appl. Phys. Lett.* **73**, 2651 (1998).
- [9] H. Ellmer, V. Repain, M. Sotto, and S. Rousset, *Surf. Sci.* **511**, 183 (2002).
- [10] B. Voigtlander, G. Meyer, and N. Amer, *Surf. Sci.* **255**, L529 (1991).
- [11] B. Voigtlander, G. Meyer, and N. Amer, *Phys. Rev. B* **44**, 10354 (1991).
- [12] H. Bulou and C. Goyhenex, *Phys. Rev. B* **65**, 45407 (2001).
- [13] J. Meyer, I. Baikie, E. Kopatzki, and R. Behm, *Surf. Sci.* **365**, L647 (1996).
- [14] B. Fischer, H. Brune, J. Barth, A. Fricke, and K. Kern, *Phys. Rev. Lett.* **82**, 1732 (1999).
- [15] V. Repain, G. Baudot, H. Ellmer, and S. Rousset, *Europhys. Lett.* **58**, 730 (2002).
- [16] V. Repain, G. Baudot, H. Ellmer, and S. Rousset, *Mat. Sci. Eng. B* **96**, 178 (2002).
- [17] G. Baudot, S. Rohart, V. Repain, H. Ellmer, Y. Girard, and S. Rousset, *Appl. Surf. Sci.* **212-213**, 360 (2003).
- [18] V. Repain, J. Berroir, S. Rousset, and J. Lecoœur, *Surf. Sci.* **447**, L152 (2000).
- [19] H. Brune, G. Bales, J. Jacobsen, C. Boragno, and K. Kern, *Phys. Rev. B* **60**, 5991 (1999).
- [20] P. Jensen, A. Barabási, H. Larralde, S. Havlin, and H. E. Stanley, *Phys. Rev. B* **50**, 15316 (1994).
- [21] J. Venables, *Phil. Mag.* **17**, 697 (1972).
- [22] J. Venables, *Phys. Rev. B* **36**, 8 (1987).

- [23] M. Bott, M. Hohage, M. Morgenstern, T. Michely, and G. Comsa, *Phys. Rev. Lett.* **76**, 1304 (1996).
- [24] H. Brune, *Surf. Sci. Rep.* **31**, 121 (1998).
- [25] J. Villain, A. Pimpinelli, L.-H. Tang, and D. Wolf, *J. Phys. I France* **2**, 2107 (1992).
- [26] C. Goyhenex and H. Bulou, *Phys. Rev. B* **63**, 235404 (2001).
- [27] Y. Liu, D. Sun, and X. Gong, *Surf. Sci.* **498**, 337 (2002).
- [28] H. Bulou, O. Lucas, M. Kibaly, and C. Goyhenex, *Comp. Mat. Sci.* **27**, 181 (2003).
- [29] J. Venables, *Physica A* **239**, 35 (1997).
- [30] A. Bortz, M. Kalos, and J. Lebowitz, *J. Comp. Phys.* **17**, 10 (1975).
- [31] J. Luo and B. Legrand, *Phys. Rev. B* **38**, 1728 (1988).
- [32] C. Bennett, in *Diffusion in Solids, Recent Developments* (A. S. Nowick and J. J. Burton, Academic, New York, 1975), p. 73.
- [33] W. C. Swope, H. C. Andersen, P. H. Berens, and K. R. Wilson, *J. Chem. Phys.* **76**, 637 (1982).
- [34] F. Ducastelle, *J. Phys. (Paris)* **31**, 1055 (1970).
- [35] G. Simmons and H. Wang, *Single Crystal Elastic Constants and Calculated Aggregates Properties* (MIT, Cambridge, 1971).
- [36] C. Kittel, *Introduction to Solid State Physics*, seventh edition ed. (John Wiley & Sons, New York, Chichester, 1996).
- [37] I. Chado, C. Goyhenex, H. Bulou, and J.-P. Bucher, to be published in *Appl. Surf. Sci.* .
- [38] E. W. Dijkstra, *Numerische Math.* **1**, 269 (1959).
- [39] H. Brune, K. Bromann, H. Röder, K. Kern, J. Jacobsen, P. Stolze, K. Jacobsen, J Nørskov, *Phys. Rev. B* **52**, R14380 (1995).
- [40] C. Ratsch, A. Seitsonen, and M. Scheffler, *Phys. Rev. B* **55**, 6750 (1997).
- [41] M. Schroeder and D. Wolf, *Surf. Sci.* **375**, 129 (1997).
- [42] C. Goyhenex, H. Bulou, J.-P. Deville, and G. Trégila, *Appl. Surf. sci.* **188**, 134 (2002).

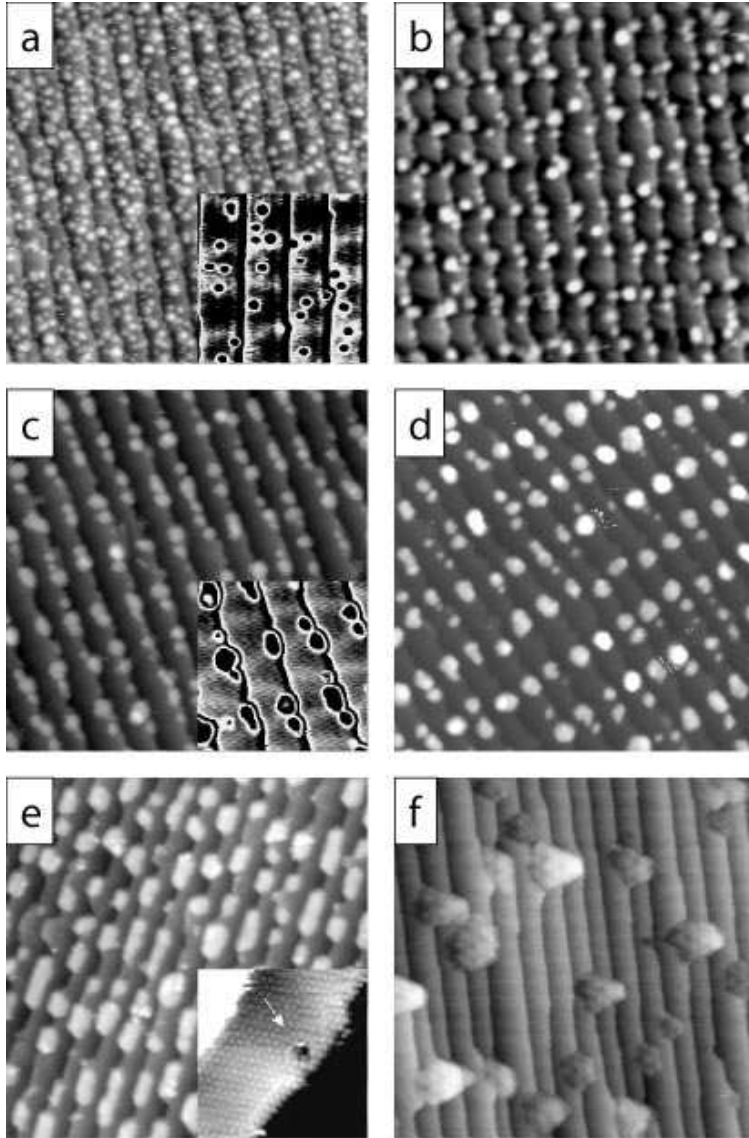


Fig. 1. STM images of cobalt deposition on Au(788) for different temperatures. Every image is 50 nm wide. a) $T = 40$ K, $\theta = 0.6$ ML: the dots are randomly distributed on the surface. (inset: 16 nm wide image of 0.005 ML Co on Au(788). The contrast due to the steps was subtracted to enhance the reconstruction (white lines).) b) 65 K, $\theta = 0.3$ ML: a rough organization is obtained. c) 95 K, $\theta = 0.3$ ML: a good organization is obtained. Dots are located at the crossing of a discommensuration line and a step edge. (inset: 16 nm wide detail of the STM image. The contrast due to the steps was subtracted in order to enhance the reconstruction.) d) 170 K, $\theta = 0.4$ ML: the good organization in c) is maintained for temperature up to 170 K. e) 300 K, $\theta = 0.3$ ML: the organization on the surface disappears and lots of inhomogeneities are seen. (inset: atomically resolved 8 nm wide image which shows an inserted nuclei of Co near the crossing of the discommensuration line and the step edge. This phenomena was observed for temperatures above 200 K.) f) 430 K, $\theta = 0.4$ ML: the dots are randomly distributed on the surface.

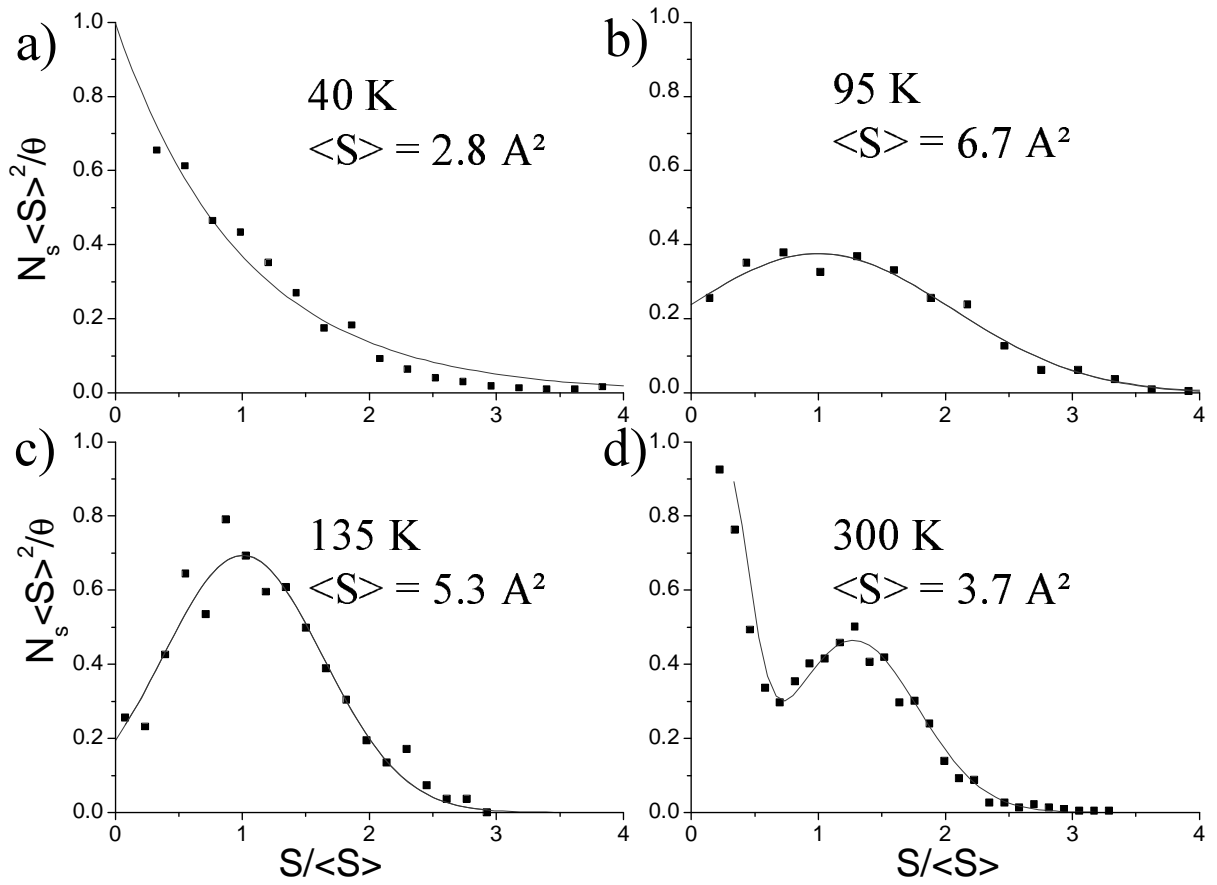


Fig. 2. Normalized size distribution of the Co clusters for different temperatures. a) $T = 40$ K, $\theta = 0.6$ ML, fitted by an exponential decay, b) $T = 95$ K, $\theta = 0.3$, fitted by a gaussian, c) $T = 135$ K, $\theta = 0.3$, fitted by a gaussian and d) $T = 300$ K, $\theta = 0.3$, fitted by a combination of a gaussian and an exponential decay.

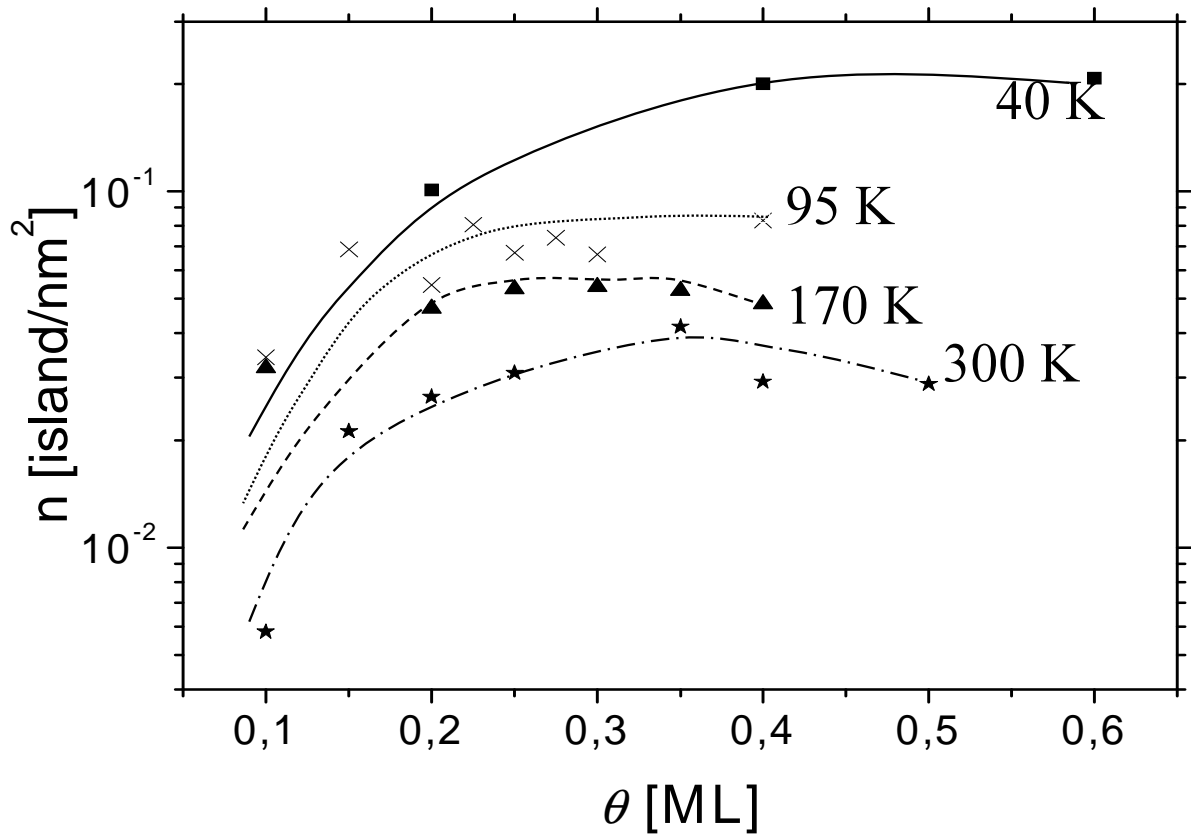


Fig. 3. The clusters density is plotted versus the Co coverage (θ) for different substrate temperatures. The dots are the experimental data and the lines are guides for the eyes.

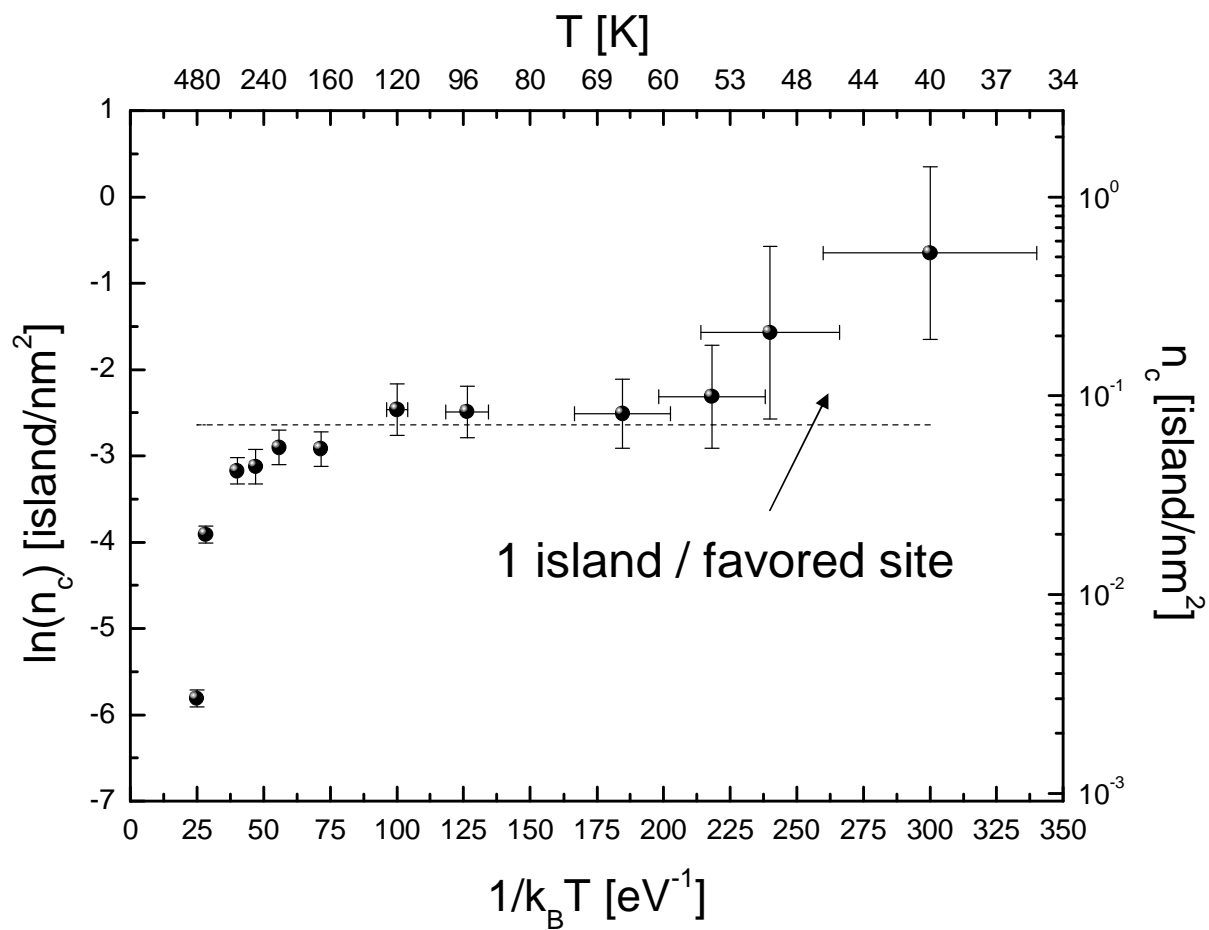


Fig. 4. Arrhenius plot of the critical clusters density evolution with temperature. The dotted line indicate the density of favored nucleation sites on Au(788).

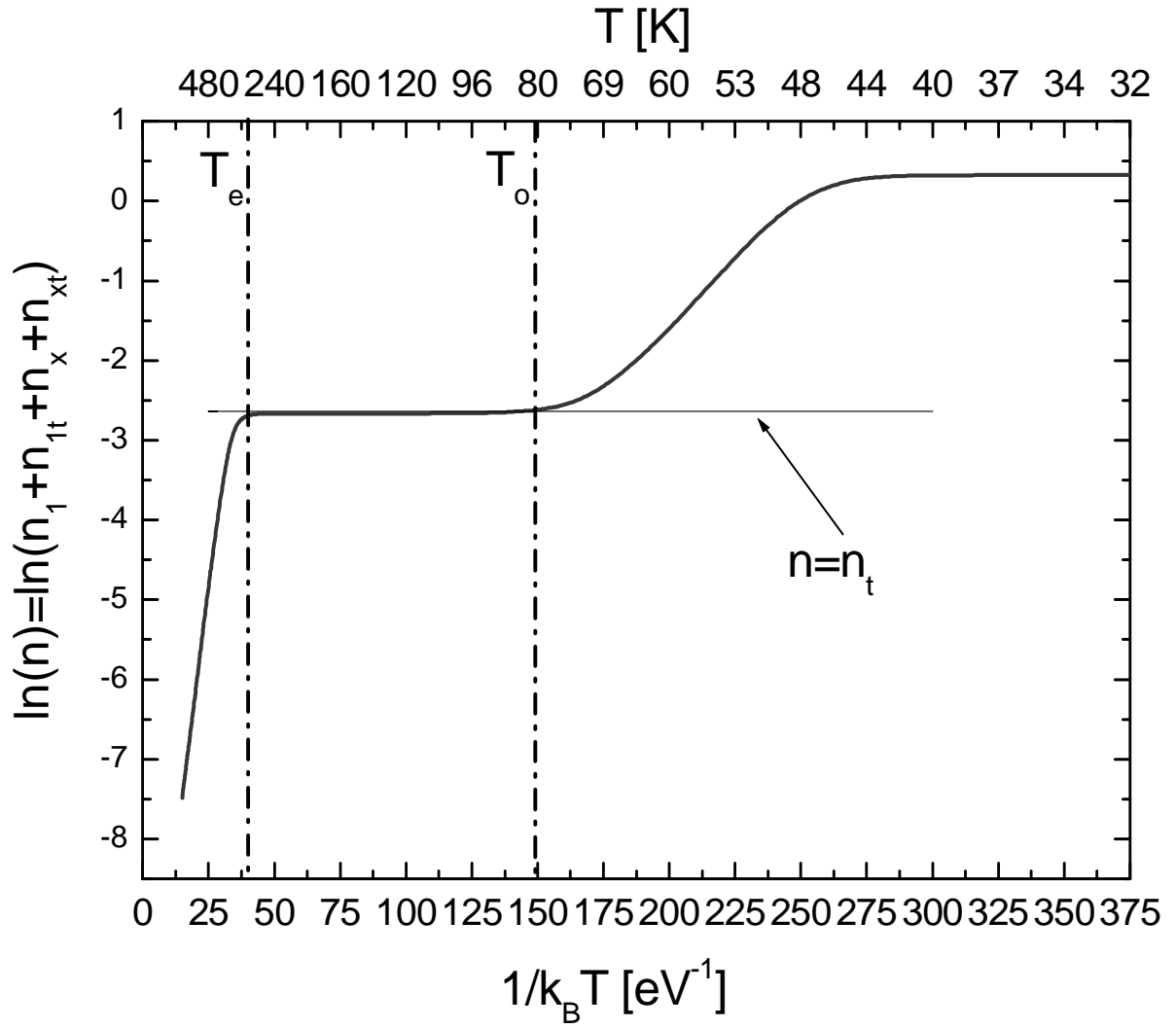


Fig. 5. Rate Equation calculation. The model take into account traps on the surface. The energy to leave the traps is set to 0.82 eV in order to fit the experimental data.

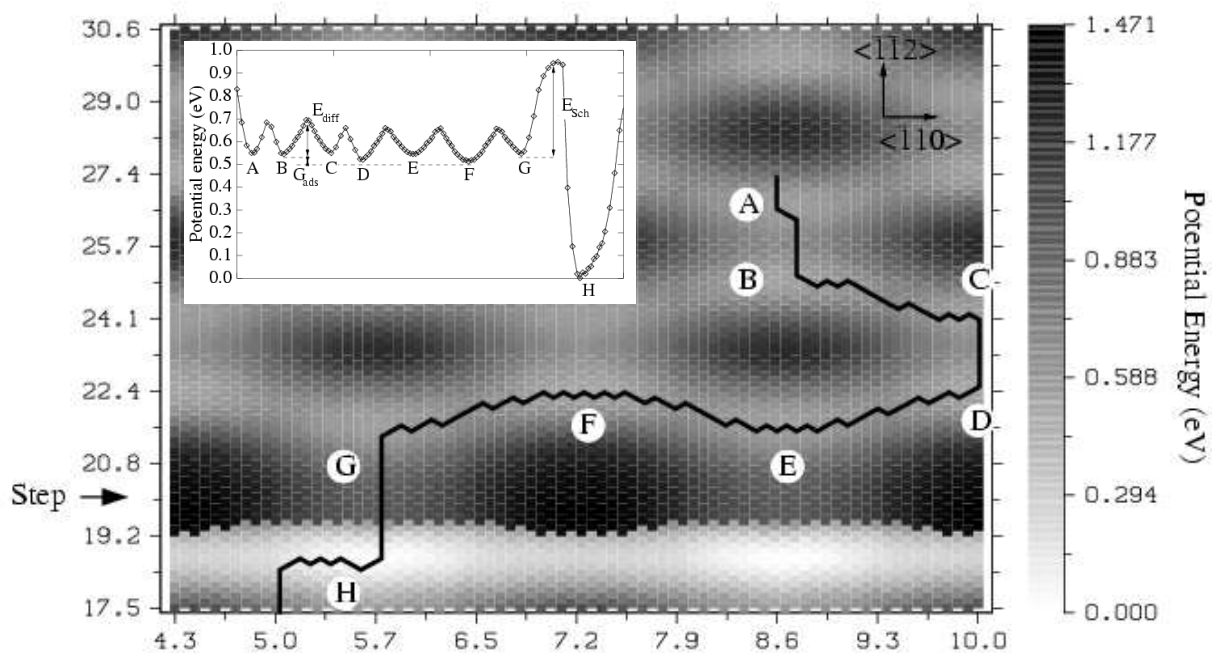


Fig. 6. Energy map of a Co adsorption. The black line is the minimum energy path from A to H.

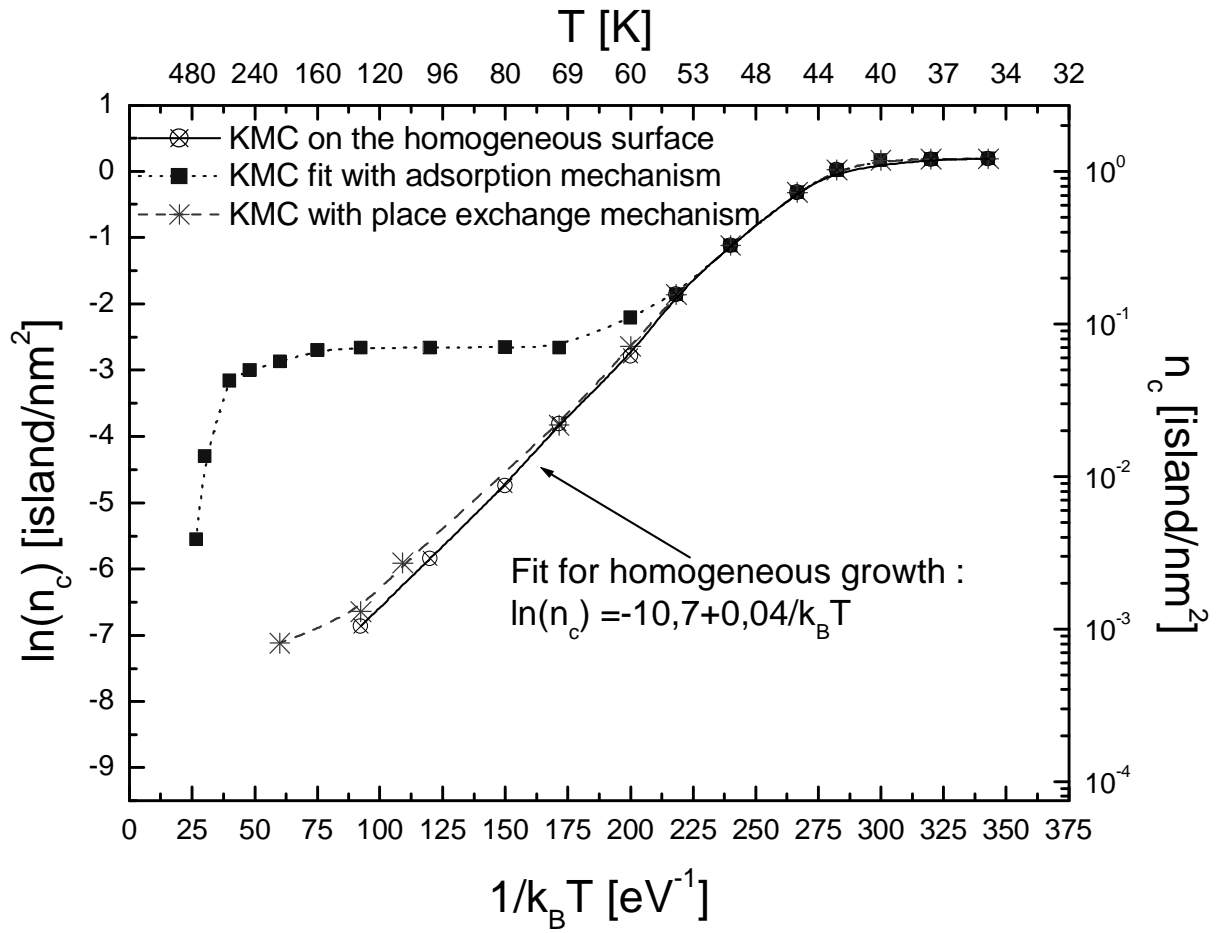


Fig. 7. KMC result for the growth with different models: (\otimes) : homogeneous surface ; (\blacksquare) : surface with favored site with the favored adsorption mechanism ; ($*$) : surface with favored site with favored place exchange mechanism.

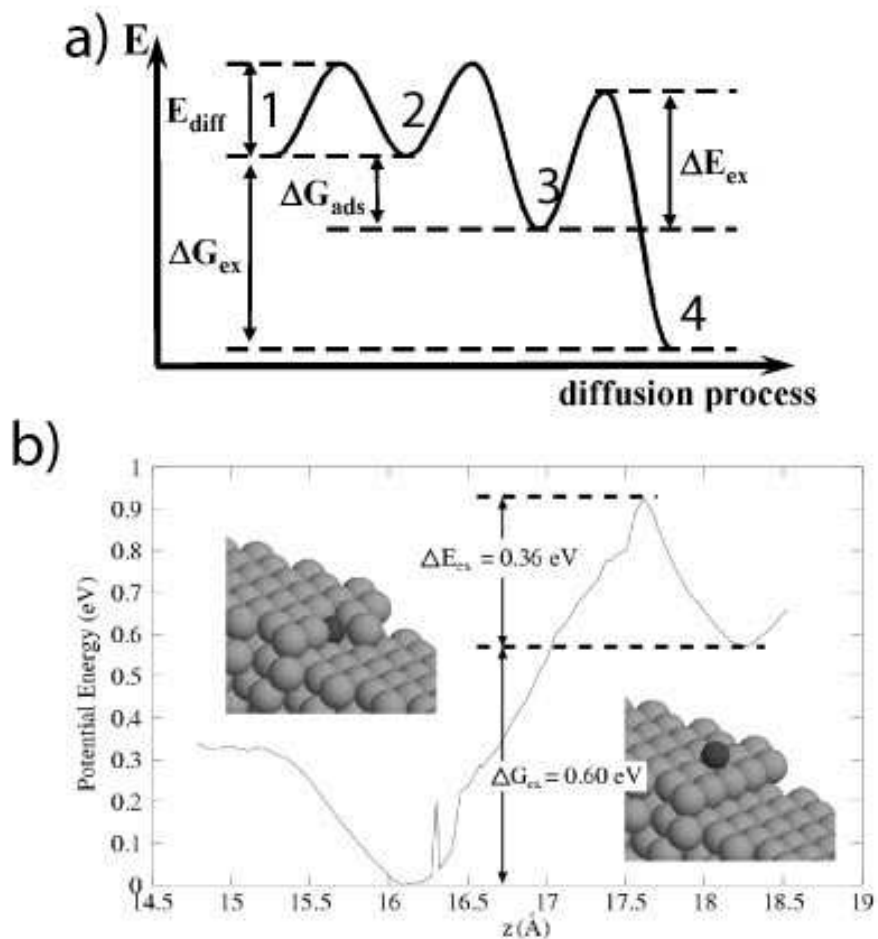


Fig. 8. a) Energetic models used in the KMC simulations for the mechanisms in the favored sites: the adatom diffuses from normal sites (1 and 2) to the favored site (3 and 4). It has first an adsorption gain ΔG_{ads} (3) with respect to the normal sites then it can exchange with a gold atom (4) jumping over the exchange barrier ΔE_{ex} . The energy gain compared to a normal site is ΔG_{ex} b) QMD calculation for the place exchange mechanism at the edge of a step.

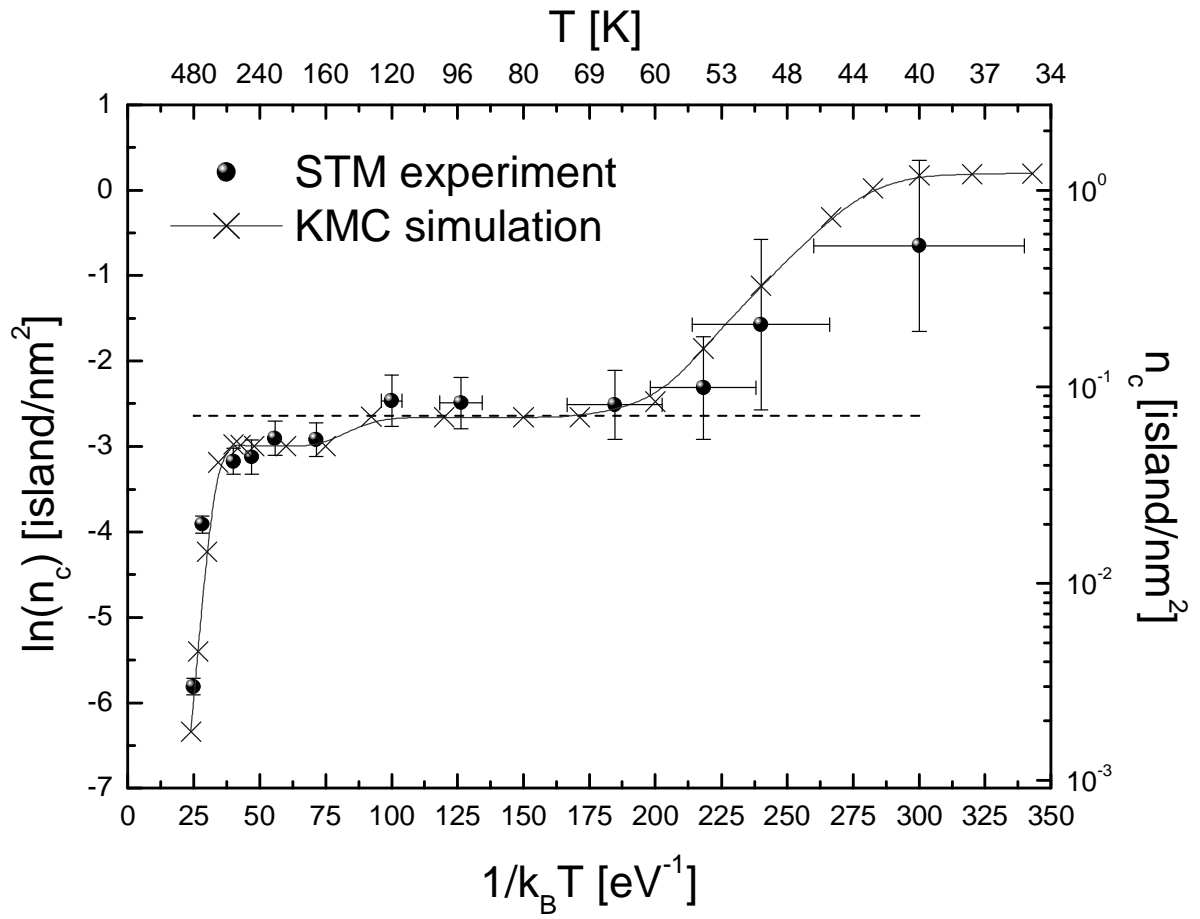


Fig. 9. KMC simulation of the growth of Co nanodots on Au(788). A good fit of the experimental data for the maximum cluster density evolution with temperature is obtained with a model combining the favored adsorption and favored place exchange mechanisms in the favored sites.

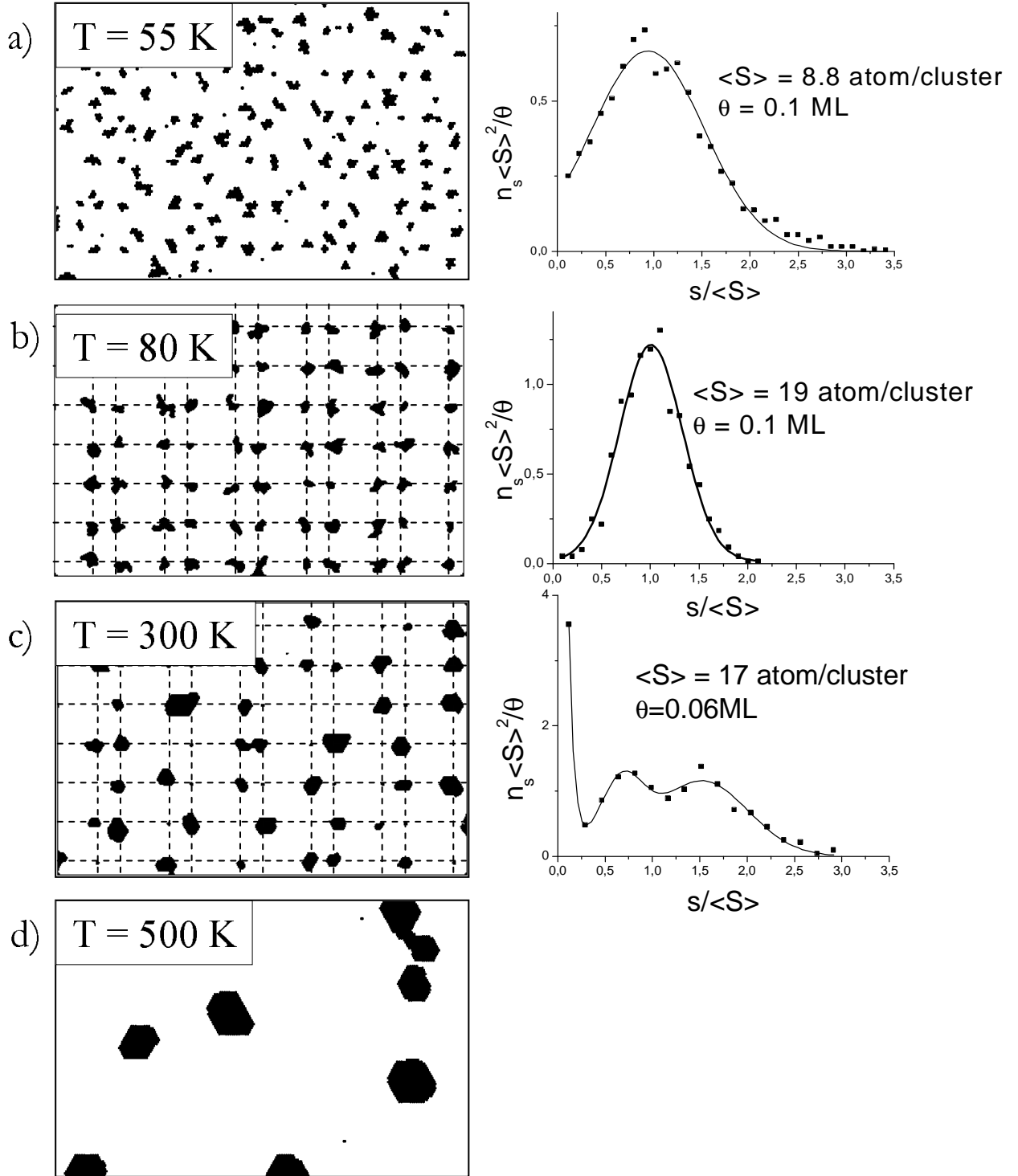


Fig. 10. KMC images and size distributions of the simulation of the growth of Co nanodots on Au(788). They show the good agreement with STM images. Images are 20×40 nm (a-c) or 50×75 nm (d) wide and are taken for a) $T = 55$ K, b) $T = 80$ K, c) $T = 300$ K and d) $T = 450$ K. In the image e), the asymmetric shape of the clusters that we have found with STM is not reproduced due to the roughness of our KMC model which does not take into account the difference between the diffusion along A and B steps.